JOURNAL OF SPACECRAFT AND ROCKETS
Vol. 43, No. 6, November–December 2006

Stochastic Launcher-Satellite Coupled Dynamic Analysis

Manuel F. Pellissetti*
Institute of Engineering Mechanics, Leopold-Franzens University, 6020 Innsbruck, Austria
Sebastiaan H. J. A. Fransen†
ESA, 2200 AG Noordwijk, The Netherlands
Helmut J. Pradlwarter‡
Institute of Engineering Mechanics, Leopold-Franzens University, 6020 Innsbruck, Austria
Adriano Calvi§
ESA, 2200 AG Noordwijk, The Netherlands
Andreas Kreis‖
Andreas Kreis Consultancies, 7212 Seewis-Dorf, Switzerland
Gerhart I. Schuëller¶
Institute of Engineering Mechanics, Leopold-Franzens University, 6020 Innsbruck, Austria
and
Michel Klein**
ESA, 2200 AG Noordwijk, The Netherlands

DOI: 10.2514/1.21154

The design and verification of spacecrafts such as satellites is supported by the results of coupled loads analyses. Herein the finite element models of the launcher and the spacecraft are typically substructured and reduced, for example, with the Craig–Bampton method, and then coupled and analyzed under various load cases occurring during launch. Inherent random uncertainties, affecting virtually all facets of the model, are traditionally dealt with by means of safety factors, with the drawback that the degree of conservatism remains unquantified. The present paper reports on a systematic, full-scale uncertainty analysis of the spacecraft-launcher assembly. Because of its versatility and its insensitivity on the number of uncertain parameters, direct Monte Carlo simulation has been used. Uncertainties in the launcher, in the spacecraft, and in the loading environment are considered separately. This allows for conclusions on the relative impact of the uncertainties on the response. The results encompass a transient load case (liftoff) and a frequency response load case (end-of-booster oscillation) and reveal that the response is particularly sensitive to uncertainties in the launcher properties, whereas the uncertainties in the loading have almost negligible impact.

Nomenclature

$\mathbf{A}$	=	Newmark integration matrices
$\mathbf{C}$	=	damping matrix
$\mathbf{F}$	=	force vector
$F_{\mathbf{X}}(\mathbf{x})$	=	joint cumulative distribution function $\mathbf{X}$
$\mathbf{f}$	=	generalized force vector
$\mathbf{G}$	=	residual flexibility matrix
$\mathbf{I}$	=	identity matrix
$\mathbf{K}$	=	stiffness matrix
$\mathbf{M}$	=	mass matrix
$\bar{\mathbf{M}}, \bar{\mathbf{C}}, \bar{\mathbf{K}}$	=	Guyan-reduced mass, damping, and stiffness matrix
n	=	Number of substructure DOFs
P	=	probability
$\mathbf{Q}(\Omega)$	=	generalized coordinates in frequency domain (amplitudes of harmonic response)
$\mathbf{q}$	=	generalized coordinates
$\mathbf{q}_p$	=	generalized coordinates associated with the fixed-interface normal modes
$\mathbf{R}$	=	reaction force
S	=	sample space of events
t	=	time
$\mathbf{u}$	=	physical coordinates (DOFs)
$\mathbf{X}$	=	random vector of uncertain model parameters
$\mathbf{x}$	=	deterministic vector of the same dimension as $\mathbf{X}$
$\mathbf{Y}$	=	vector of random response quantities of interest
$\mathbf{y}$	=	deterministic vector of the same dimension as $\mathbf{Y}$
θ	=	random event
$\mathbf{\Lambda}$	=	diagonal matrix of natural frequencies
μ	=	mean of a random variable
σ	=	standard deviation of a random variable
$\boldsymbol{\phi}_{ij}$	=	constraint modes
$\boldsymbol{\varphi}_{ip}$	=	natural modes for fully constrained interface
$\mathbf{\Psi}$	=	Craig–Bampton transformation matrix
Ω	=	excitation frequency
$\mathbf{0}$	=	matrix of zeros

Subscripts

b	=	union of all j sets, that is, of all interface DOFs
CB	=	Craig–Bampton
D	=	dimension of random vector $\mathbf{X}$, that is, number of uncertain model parameters
d	=	truncated modes

Received 18 November 2005; revision received 7 April 2006; accepted for publication 15 April 2006.

*Postdoctoral Fellow, Institute of Engineering Mechanics, Technikerstrasse 13; Mechanik@uibk.ac.at.
†Consultant, Structures Section, AOES Group B.V.; bas.fransen@aoes.com. Professional Member AIAA
‡Associate Professor, Institute of Engineering Mechanics.
§Project Manager, Structures Section TEC-MCS, ESA/European Space Research and Technology Center, P.O. Box 299; adriano.calvi@esa.int.
‖Consultant, Crestacalva 150; andreas.kreis@akrs.ch. Professional Member AIAA.
¶Professor and Chair, Institute of Engineering Mechanics.
**Head of Thermal and Structures Division, ESA/European Space Research and Technology Center, P.O. Box 299; michel.klein@esa.int.

h = current step in the Newmark integration
i = interior DOF
j = interface DOF
l = index of a single component of random vector $\mathbf{X}$
M = total number of MCS runs
m = index of a single MCS run
p = fixed-interface normal modes

Superscripts

(k) = kth substructure
(L) = total number of substructures
MA = mode acceleration

I. Introduction

LAUNCHER-PAYLOAD coupled dynamic analysis is employed as a tool for payload dimensioning and verification and is carried out as part of the mission analysis. The objective is the computation of the payload mechanical environment due to dynamic loads occurring at particular instants of time during launch [1]. Although the high resolution of refined finite element (FE) meshes potentially improves the quality of the predictions retrieved from coupled dynamic analyses, the great amount of assumptions during the construction of the model and the uncertainties concerning its parameters tend to counteract the potential gain in precision.

Practitioners help themselves by applying safety factors [2,3], a fact that demonstrates that the presence of uncertainties is acknowledged; however, this approach falls short of providing a truly rational basis for quantifying and managing the unavoidable and often significant uncertainties [4]. Such a basis is instead afforded by probability theory, with its rich and well-developed concepts, which are supported by numerous efficient algorithms for their computational implementation [5].

Preliminary European studies on the feasibility of statistical, Monte Carlo method based, spacecraft-launcher coupled load analyses (CLA) were first performed in the early 1990s. Reference [6] can be viewed as a preliminary step in the direction taken by the present papers, as it reports results of the scatter in the CLA response induced by the uncertainty in the spacecraft's properties. The latter is, however, introduced in a heuristic manner, by modeling the modal properties, natural frequencies and effective modal masses, directly as uniformly distributed random variables, treating the mathematical model of the spacecraft as a black box. A similar approach has recently been adopted in [7], in which the modal properties of the subsystems are modeled as random variables, to estimate response statistics of uncertain structures in the midfrequency domain. With respect to [6], it should also be noted that there the damping was assumed to be completely deterministic and the same applied to the model of the launcher and the loading. Furthermore, the response of the coupled system was not evaluated by means of a full-scale CLA.

In contrast to this earlier work, in the present paper the influence of uncertainties in the payload, the launcher, and in the loading is analyzed systematically, by propagating the uncertainties present in each of these three major components of the mathematical model separately through the complete CLA. The methodology used to propagate the uncertainties in the model to the response is direct Monte Carlo simulation (DMCS), because this technique is unmatched when it comes to versatility and generality. In fact, this method is independent of the number of random input parameters, which is an essential characteristic for the application dealt with in the present paper, because the number of random variables on the input side is extremely high. This fact is a consequence of the fundamental assumption made in the probabilistic modeling process, namely, that the vast majority of the parameters of the FE model are uncertain and hence are to be modeled as random variables. For the sake of convenience, the exact opposite is usually done, namely, a small subset of the parameters are defined as random variables, typically those which are expected to be most influential with respect to the response. Such an approach is sometimes, but certainly not always, justified, and it has invariably the great advantage of facilitating the application of methods whose performance is sensitive to the number of random variables, such as the response surface method. For complex structures it is, however, quite difficult and error prone to state a priori which parameters are most influential. In fact, when multiple response quantities of the analysis are considered, different, conflicting sets of parameters might be influential. Based on these arguments, in this study the majority of parameters of the FE model have been modeled as random variables. The validity of the arguments is supported by the results of the study, which demonstrate that different response quantities are most sensitive to very different parameters.

Two load cases, for which the coupled loads analysis is typically performed during spacecraft design and testing, have been considered in the present work, namely, the liftoff (LO) and the so-called end-of-booster pressure oscillation (EBP) load case. For each of these load cases three sets of MC simulations, with 1500 samples each, have been performed: one in which the parameters of the satellite FE model are uncertain, one in which the parameters of the launcher FE model are uncertain, and one in which some of the loading parameters are uncertain. The reasoning behind looking at the uncertainties in the satellite, the launcher, and the loading separately is that this way one can assess the relative importance of the uncertainties in these three quite distinct aspects of the model. As the results of the full-scale coupled loads analysis of the Ariane 5 launcher coupled with the INTEGRAL satellite of European Space Agency (ESA) show, the effects of the uncertainty in each of these three areas of the model are quite different in magnitude. This observation shows that the separate consideration was justified, because it avoids loss of information. Indeed, had the uncertainties in all sources been modeled simultaneously, then the response scatter due to the launcher uncertainties would have dominated and obscured the scatter due to satellite and loading uncertainties.

II. Method of Analysis

A. Coupled Dynamic Analysis Method

1. Substructuring

To reduce the computational effort for the dynamic analysis of large FE models, it is common practice to apply substructuring techniques. The method applied in the analyses presented in this paper is the popular Craig–Bampton method [8]. In this method for each substructure the vector of physical degrees of freedom (DOFs) $\mathbf{u}$ is subdivided in the interface DOFs $\mathbf{u}_j$ and the interior DOFs $\mathbf{u}_i$, leading to the following equations of motion for the substructure in partitioned form [9]:

$$\begin{bmatrix} \mathbf{M}_{jj} & \mathbf{M}_{ji} \\ \mathbf{M}_{ij} & \mathbf{M}_{ii} \end{bmatrix} \begin{bmatrix} \ddot{\mathbf{u}}_j \\ \ddot{\mathbf{u}}_i \end{bmatrix} + \begin{bmatrix} \mathbf{K}_{jj} & \mathbf{K}_{ji} \\ \mathbf{K}_{ij} & \mathbf{K}_{ii} \end{bmatrix} \begin{bmatrix} \mathbf{u}_j \\ \mathbf{u}_i \end{bmatrix} = \begin{bmatrix} \mathbf{F}_j \\ \mathbf{F}_i \end{bmatrix} + \begin{bmatrix} \mathbf{R}_j \\ \mathbf{0}_i \end{bmatrix} \quad (1)$$

where F_j, F_i are applied forces and R_j are reaction forces at the interfaces. Damping is omitted in this formulation for simplicity, but has been included in the analyses presented in Sec. III.

The physical coordinates $\mathbf{u}$ are expressed in terms of generalized coordinates $\mathbf{q}$, with the following transformation, $\mathbf{u} = \mathbf{\Psi}\mathbf{q}$, where

$$\mathbf{\Psi} = \begin{bmatrix} \mathbf{I}_{jj} & \mathbf{0}_{jp} \\ \boldsymbol{\phi}_{ij} & \boldsymbol{\varphi}_{ip} \end{bmatrix} \quad \text{and} \quad \mathbf{q} = [\mathbf{u}_j \mathbf{q}_p]^T \quad (2)$$

Here $\mathbf{u}_j$ are the interface DOFs and $\mathbf{q}_p$ contains a subset of the modal coordinates which are associated with the normal modes $\boldsymbol{\varphi}_{ip}$ of the component, assuming a fully constrained interface. The columns of $\boldsymbol{\phi}_{ij}$ are the constraint modes, obtained by imposing in turn a unit displacement to each interface DOF, while constraining the other interface DOFs.

Substituting Eq. (2) in Eq. (1) and premultiplying with $\mathbf{\Psi}^T$ reduces the set of equations,

$$\begin{bmatrix} \bar{\mathbf{M}}_{jj} & \mathbf{M}_{jp} \\ \mathbf{M}_{pj} & \mathbf{M}_{pp} \end{bmatrix} \begin{bmatrix} \ddot{\mathbf{u}}_j \\ \ddot{\mathbf{q}}_p \end{bmatrix} + \begin{bmatrix} \bar{\mathbf{K}}_{jj} & \mathbf{0}_{jp} \\ \mathbf{0}_{pj} & \mathbf{\Lambda}_{pp} \end{bmatrix} \begin{bmatrix} \mathbf{u}_j \\ \mathbf{q}_p \end{bmatrix} = \begin{bmatrix} \mathbf{F}_j + \boldsymbol{\phi}_{ij}^T \mathbf{F}_i \\ \boldsymbol{\varphi}_{ip}^T \mathbf{F}_i \end{bmatrix} + \begin{bmatrix} \mathbf{R}_j \\ \mathbf{0}_p \end{bmatrix} \tag{3}$$

where $\bar{\mathbf{M}}$ and $\bar{\mathbf{K}}$ are the Guyan-reduced (statically reduced) matrices with respect to the interface DOFs. The interface reaction forces $\mathbf{R}_j$ are unknown, but cancel out when the equations of the various components are combined to the global system of equations,

$$\begin{bmatrix} \bar{\mathbf{M}}_{bb} & \mathbf{M}_{jp}^{(1)} & \mathbf{M}_{jp}^{(2)} & \cdots & \mathbf{M}_{jp}^{(L)} \\ & \mathbf{I}_{pp}^{(1)} & \mathbf{0} & \cdots & \mathbf{0} \\ & & \mathbf{I}_{pp}^{(2)} & \ddots & \vdots \\ & & & \ddots & \mathbf{0} \\ \text{sym} & & & & \mathbf{I}_{pp}^{(L)} \end{bmatrix} \begin{bmatrix} \ddot{\mathbf{u}}_b \\ \ddot{\mathbf{q}}_p^{(1)} \\ \ddot{\mathbf{q}}_p^{(2)} \\ \vdots \\ \ddot{\mathbf{q}}_p^{(L)} \end{bmatrix} + \begin{bmatrix} \bar{\mathbf{K}}_{bb} & \mathbf{0} & \cdots & \cdots & \mathbf{0} \\ & \mathbf{\Lambda}_{pp}^{(1)} & \mathbf{0} & \cdots & \mathbf{0} \\ & & \mathbf{\Lambda}_{pp}^{(2)} & \ddots & \vdots \\ & & & \ddots & \mathbf{0} \\ \text{sym} & & & & \mathbf{\Lambda}_{pp}^{(L)} \end{bmatrix} \begin{bmatrix} \mathbf{u}_b \\ \mathbf{q}_p^{(1)} \\ \mathbf{q}_p^{(2)} \\ \vdots \\ \mathbf{q}_p^{(L)} \end{bmatrix} = \begin{bmatrix} \mathbf{F}_b \\ \mathbf{f}_p^{(1)} \\ \mathbf{f}_p^{(2)} \\ \vdots \\ \mathbf{f}_p^{(L)} \end{bmatrix} \tag{4}$$

The b set of DOFs, indicated by the subscript b in the quantities $\bar{\mathbf{M}}_{bb}$, $\bar{\mathbf{K}}_{bb}$, $\ddot{\mathbf{u}}_b$, $\mathbf{u}_b$, and $\mathbf{F}_b$ is the union of the j sets of all components, that is, of the interface DOFs of all the substructures together. The vector $\mathbf{F}_b$ denotes the external forces on the interfaces and $\mathbf{f}_p^{(k)}$ are the generalized forces associated with the kth substructure.

2. Mode Acceleration Method

The loss of accuracy induced by the truncation of the full component mode matrix can be reduced by adding a correction term to the internal displacements obtained with the modal superposition [9,10],

$$\mathbf{u}_i^{\mathrm{MA}} = \mathbf{u}_i + \mathbf{G}_d \left[\mathbf{F}_i - \left(\mathbf{M}_{ij} - \mathbf{M}_{ii} \mathbf{K}_{ii}^{-1} \mathbf{K}_{ij} \right) \ddot{\mathbf{u}}_j \right] \tag{5}$$

Here, $\mathbf{G}_d$ is the residual flexibility matrix of the truncated modes $\boldsymbol{\varphi}_{id}$ and is given by

$$\mathbf{G}_d = \boldsymbol{\varphi}_{id} \mathbf{\Lambda}_{dd}^{-1} \boldsymbol{\varphi}_{id}^T = \mathbf{K}_{ii}^{-1} \left[\mathbf{I}_{ii} - \mathbf{M}_{ii} \boldsymbol{\varphi}_{ip} \boldsymbol{\varphi}_{ip}^T \right] \tag{6}$$

Hence, the correction consists of the static displacement associated with the truncated modes, due to the internal forces $\mathbf{F}_i$ and the acceleration of the interface $\ddot{\mathbf{u}}_j$.

3. Coupled Load Analysis: Direct Transient Analysis

Rewriting the matrix Eq. (4) in a compact form, including damping, one obtains

$$\mathbf{M}_{\mathrm{CB}} \ddot{\mathbf{q}}_{\mathrm{CB}}(t) + \mathbf{C}_{\mathrm{CB}} \dot{\mathbf{q}}_{\mathrm{CB}}(t) + \mathbf{K}_{\mathrm{CB}} \mathbf{q}_{\mathrm{CB}}(t) = \mathbf{F}_{\mathrm{CB}}(t) \tag{7}$$

where the generalized forces $\mathbf{F}_{\mathrm{CB}}(t)$ give rise to the transient response $\mathbf{q}_{\mathrm{CB}}(t)$. Applying a Newmark-type time integration method leads to

$$\mathbf{A}_1 \mathbf{q}_{\mathrm{CB},h+1} = \mathbf{A}_2 + \mathbf{A}_3 \mathbf{q}_{\mathrm{CB},h} + \mathbf{A}_4 \mathbf{q}_{\mathrm{CB},h-1} \tag{8}$$

where $\mathbf{A}_1$, $\mathbf{A}_2$, $\mathbf{A}_3$, and $\mathbf{A}_4$ are functions of $\mathbf{M}_{\mathrm{CB}}$, $\mathbf{C}_{\mathrm{CB}}$, and $\mathbf{K}_{\mathrm{CB}}$, as well as of the time step size Δt and the exciting force. The subscript h denotes the current step in the integration process. The exact values of the system matrices depend on the tuning parameters of the selected integration scheme.

4. Coupled Load Analysis: Direct Frequency Response Analysis

Consider the case in which the generalized forces of the assembled Craig–Bampton system in Eq. (4) are harmonic with varying excitation frequency Ω. Adopting a compact notation as in Eq. (7) the equation of motion reads

$$\mathbf{M}_{\mathrm{CB}} \ddot{\mathbf{q}}_{\mathrm{CB}}(t) + \mathbf{C}_{\mathrm{CB}} \dot{\mathbf{q}}_{\mathrm{CB}}(t) + \mathbf{K}_{\mathrm{CB}} \mathbf{q}_{\mathrm{CB}}(t) = \mathbf{F}_{\mathrm{CB}}(\Omega) e^{i\Omega t} \tag{9}$$

where $\mathbf{q}_{\mathrm{CB}}(t)$ is the complex Craig–Bampton response vector. Assuming a solution of the form,

$$\mathbf{q}_{\mathrm{CB}}(t) = \mathbf{Q}_{\mathrm{CB}}(\Omega) e^{i\Omega t} \tag{10}$$

and substituting in Eq. (9) leads to the following system of equations:

$$(-\Omega^2 \mathbf{M}_{\mathrm{CB}} + i\Omega \mathbf{C}_{\mathrm{CB}} + \mathbf{K}_{\mathrm{CB}}) \mathbf{Q}_{\mathrm{CB}}(\Omega) = \mathbf{F}_{\mathrm{CB}}(\Omega) \tag{11}$$

The frequency response can then be evaluated by varying the excitation frequency Ω in Eq. (11) over the range of interest and directly solving the complex system of linear equations for $\mathbf{Q}_{\mathrm{CB}}(\Omega)$.

B. Monte Carlo Simulation

The objective of the present study was to assess the impact of the uncertainties on the predictions of the CLA, by using a probabilistic approach. In this framework, the uncertain quantities of the numerical model can be formally collected in a random vector,

$$\mathbf{X} = [X_1 X_2 \cdots X_l \cdots X_D], \qquad X_l = X_l(\theta), \qquad \theta \in S \tag{12}$$

where D denotes the dimension of the random vector $\mathbf{X}$. The latter is fully characterized by its joint cumulative distribution function (CDF),

$$F_{\mathbf{X}}(\mathbf{x}) = P[X_1 \le x_1, X_2 \le x_2, \ldots, X_D \le x_D] \tag{13}$$

where $\mathbf{x} = [x_1 x_2 \cdots x_D]$ are deterministic. The randomness in the parameters propagates to the system matrices [e.g., Eq. (7)] and hence to the response

$$\begin{gathered} \mathbf{M}_{\mathrm{CB}} = \mathbf{M}_{\mathrm{CB}}(\theta), \qquad \mathbf{C}_{\mathrm{CB}} = \mathbf{C}_{\mathrm{CB}}(\theta), \qquad \mathbf{K}_{\mathrm{CB}} = \mathbf{K}_{\mathrm{CB}}(\theta) \\ \mathbf{F}_{\mathrm{CB}} = \mathbf{F}_{\mathrm{CB}}(\theta) \Rightarrow \mathbf{q}_{\mathrm{CB}} = \mathbf{q}_{\mathrm{CB}}(\theta) \end{gathered} \tag{14}$$

The objective of the uncertainty analysis is to estimate the CDF $F_{\mathbf{Y}}(\mathbf{y})$ of the response quantities of interest $\mathbf{Y} = \mathbf{Y}(\mathbf{q}_{\mathrm{CB}}(\theta))$.

It is well known that with the exception of the distribution tails direct Monte Carlo simulation is very efficient, as with a relatively modest number of samples the CDF can be quantified. The convergence can be assessed by means of statistical error estimators. Furthermore DMCS is particularly straightforward to implement, as it does not require access to the source code of the numeric solver. This is a critical advantage in the context of large scale industrial applications, because these are usually analyzed with general-purpose finite element packages which cannot be modified.

Because the responses of interest in this study were computed over an extended frequency range or over time intervals, the CDF was represented at discrete probability levels, in terms of fractiles. The response fractile y_P for a given response Y and a given probability level P is approximated as follows. Let $\{Y_m\}_{m=1}^M$ be the ensemble of responses obtained by performing M DMCS runs and let $\{\hat{Y}_m\}_{m=1}^M$ contain the elements of $\{Y_m\}$, but in increasing order,

$$\left\{ \hat{Y}_m \right\}_{m=1}^M, \qquad \hat{Y}_1 \le \hat{Y}_2 \le \cdots \le \hat{Y}_M \tag{15}$$

Then,

$$y_P \approx \hat{Y}_{M_P}, \qquad \begin{gathered} M_P = \mathrm{round}[P \cdot (M+1)] \\ 1 \le M_P \le M \end{gathered} \tag{16}$$

where the operator round $[\cdot]$ rounds the argument to the nearest integer.

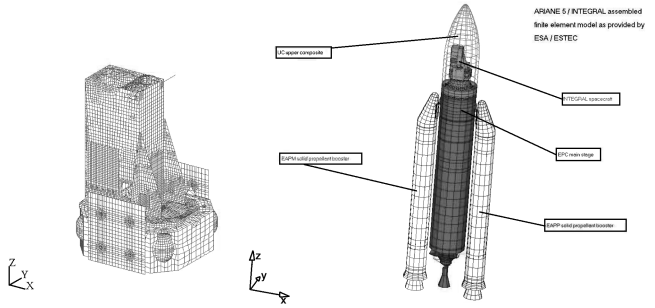

Fig. 1 FE models of INTEGRAL satellite (left) and Ariane 5 launcher (right) (Courtesy of ESA).

III. Uncertainty Analysis of Coupled System Launcher Satellite

A. Finite Element Models

Two finite element models are used in this study. The first one concerns the research satellite INTEGRAL (INTErnational Gamma Ray Astrophysics Laboratory) [11]. The second one is ESA's model of the Ariane-5 launcher [12], subdivided into four substructures. Both models are shown in Fig. 1.

The INTEGRAL FE model has roughly 120,000 DOF, with a total mass of 3800 kg. A finer mesh has been used in this case as it is also used for the purpose of stress analysis. The instruments have been partly reduced to Craig–Bampton (CB) and Guyan [13] reduced models and are included in the FE model. The model is reduced to a CB model of approximately 330 DOF, which is only 0.3% of the original FE model size.

The Ariane-5 FE model has approximately 33,000 DOF and a total mass of 745,000 kg during the liftoff load case and 277,000 kg during the booster oscillation load case. The Ariane-5 FE model can be subdivided into four substructures:

1) étage d'acceleration à poudre − (EAP− or EAPM)
2) étage d'acceleration à poudre + (EAP+ or EAPP)
3) étage à propulsion cryotechnique (EPC)
4) upper composite (UC)

The solid rocket booster stages have been modeled with shell elements and with solid elements. The latter are used to model the solid propellant. The EPC FE model also contains fluid models to take into account the sloshing of the liquid oxigen (LOX) and liquid hydrogen (LH2) in the upper and lower tank, respectively. The fluid models have been defined on the basis of boundary elements [14]. The fluid mass and stiffness matrices are added to the corresponding tank wall and free fluid surface. The sloshing frequencies are of the order of [0.5:3] Hz. The upper composite FE model is composed of the vehicle equipment bay (VEB) control unit, and storable propellant upper stage (EPS) propulsion unit, a payload adapter, and a fairing. The increase in stiffness due to the pressurization of the EPC tanks and EAP boosters has been taken into account by the addition of geometric stiffness to the respective substructure stiffness matrices. Reducing the complete Ariane-5 FE model including payload leads to a CB system of equations with approximately 700 DOF, that is 0.5% of the FE-system size.

B. Coupled Loads Analysis Launcher Satellite

The two analyzed load cases, namely, the liftoff and the thrust (pressure) oscillation load cases, are depicted in Fig. 2. The dynamic loads during liftoff are composed of the thrust forces (longitudinal) and the blast wave pressure (lateral) which emerges from the exhaust ducts of the channels that lead away the booster combustion gases. The pressure oscillation case occurs at approximately 110 s after liftoff and is introduced by the second acoustic cavity mode in the boosters. The acoustic modes are assumed to be out of phase and thus cause a lateral excitation at the spacecraft interface.

The meaning of the spacecraft mechanical environment is clarified in Fig. 3. Of main interest are the interface accelerations and forces, which can be used to derive the equivalent sine spectrum and the center of gravity (COG) net accelerations. In addition one might be

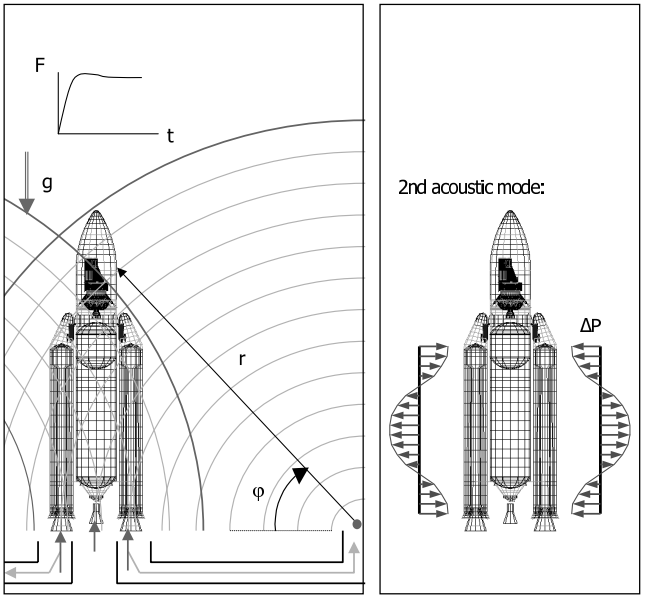

a) Liftoff **b) Thrust oscillations**

Fig. 2 A selection of Ariane-5 load cases.

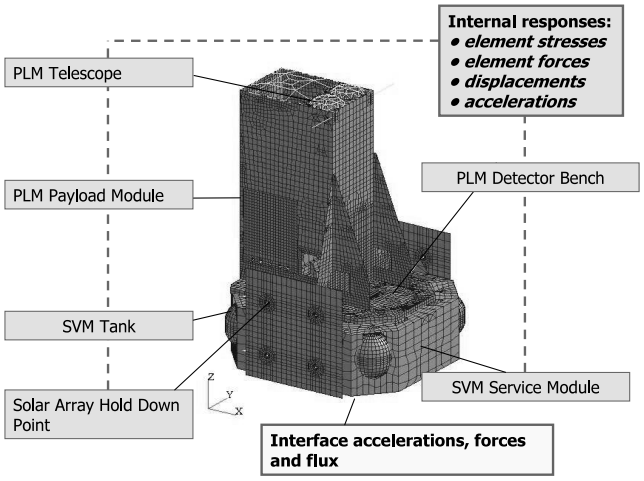

Fig. 3 The mechanical environment of the spacecraft [service module (SVM) and payload module (PLM)].

interested in the computation of internal responses to verify the structural integrity of specific instruments on board of the spacecraft. The computed responses can then be employed within the design, verification, and test phases of the spacecraft concerned.

The launcher-payload coupled dynamic analysis procedure can be subdivided into two loops, as depicted in Fig. 4. The first loop is associated with the generation of the reduced substructure models on the basis of the CB method [8]. Generally this process is referred to as component mode synthesis (CMS). For the Ariane-5/Integral

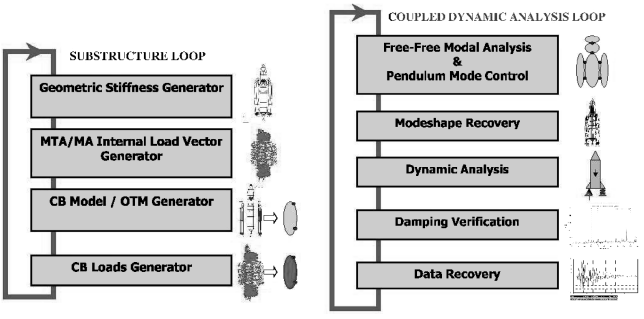

Fig. 4 Coupled dynamic analysis process.

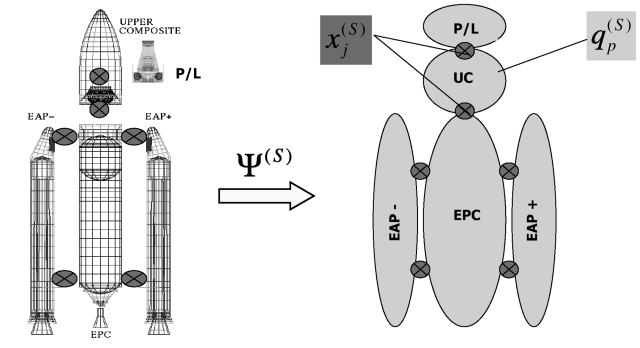

MODEL	NDOF
UC	13068
EPC	6571
EAP-	6657
EAP+	6657
P/L	119067
SYSTEM (I/F merged)	151666

MODEL	NDOF	REDUCTION
UC	533	4.1%
EPC	207	3.1%
EAP-	41	0.6%
EAP+	41	0.6%
P/L	326	0.3%
SYSTEM (I/F merged)	690	0.5%

Fig. 5 Substructure reduction and assembly.

substructures this reduction process is visualized in Fig. 5. If specific output is requested for the substructure, then output transformation matrices (OTMs) shall be computed as well [15]. In case the dynamic loads of the flight events to be studied are applied to the substructure under consideration, also the transformation of the loads to CB generalized loads is performed. The second loop is related to the dynamic analysis with the reduced CB system as depicted on the right side of Fig. 5. To identify the modal content of the system a modal analysis is run followed by the optional recovery of the physical mode shapes. During this modal analysis of the free–free CB system, a control matrix is computed such that the pendulum modes are enforced to zero-eigenvalue rigid body modes. Because the Ariane-5 model contains fluid models for the liquid propellants, which lead to pendulum modes, this step has to be performed [16]. The next step is the dynamic analysis, either in the time or in the frequency domain, followed by the data recovery of physical responses. Optionally, the system damping can be verified for the configuration used in the dynamic analysis. This loop is repeated for each flight event.

In terms of computational cost the reduction of the substructure FE models to CB models is the most demanding step, because the Lanczos process is $\mathcal{O}(n^3)$ in terms of floating point operations [17]. Here n is equal to the number of substructure DOF. The cost of any analysis with the reduced system can be neglected compared to the cost of the reduction process as the number of DOF has been reduced dramatically. This is evident when one compares the FE system and CB system size given in the tables in Fig. 5.

C. Probabilistic Model

For complex FE models, such as those dealt with in the present study, it is very hard to identify a priori the uncertain parameters with great impact on the response quantities of interest and those with negligible impact. Furthermore, various response quantities (stresses, interface forces, accelerations) at various locations of the structure are relevant, with different sensitivities. In addition, limited specific information on the degree of uncertainty associated with the various parameters is available.

To ensure as great a generality as possible, a conservative approach has been taken and as many FE model parameters as possible have been treated as random variables. This way the risk of ignoring the uncertainties in parameters with a great impact on the response is minimized.

This generality, however, leads to an unusually large number of random variables, approximately 1300 for both the satellite and the launcher. The levels of variability are selected on the basis of data available in the literature [2,3,18,19]. Table 1 shows the assumptions made for the magnitude of the scatter in the uncertain finite element model parameters. For instance, for Young's moduli of isotropic materials the coefficient of variation (COV) σ/μ, where μ is the mean and σ is the standard deviation was assumed to be 8%. The assumed coefficients of variation range from 4 to 12%.

The mean values were set equal to the nominal values of the deterministic FE model. The probability distribution of the random properties was mostly Gaussian, with the exception of the damping. This assumption is sufficiently accurate given the lack of hard data. Because of the small coefficients of variation, the probability of occurrence of negative values for properties such as Young's modulus is practically zero. However, this does not apply to the damping, which is usually affected by greater uncertainty. In this case a log-normal distribution with a COV of 20% for modal damping and of 25% for structural damping has been assumed.

It should be noted that in this study the stochastic finite element method has not been used, that is, the spatial correlation of the uncertain parameters has not been taken into account. The main reason for this is that statistical information on the correlation distance of properties is extremely scarce.

Concerning the uncertainties in the loading, the related assumptions are stated in Secs. III.F (liftoff) and III.G (end-of-booster pressure).

D. Remarks on Implementation Issues

In the stochastic launcher-payload coupled dynamic analysis study reported in this paper, two software codes were employed. The code FE-RV [20] controls the Monte Carlo simulation; based on an input file in which the user specifies the probability distributions of the uncertain model parameters the code generates random realizations of the parameters, automatically edits the input files of the deterministic FE code, and drives the FE solver to evaluate the corresponding response realizations. The software is a collection of PERL modules and scripts and is based on earlier versions, which are entirely FORTRAN based [21,22].

The CLA Toolbox [23], which operates in combination with the commercial FE package MSC.Nastran™, is a collection of direct matrix abstraction programming (DMAP) procedures which run with the various solution sequences of MSC.Nastran and has been developed within ESA.

E. Modal Analysis

1. *General Remarks*

The first step in the CLA loop is the modal analysis of the CB-reduced system, as shown in the right portion of Fig. 4. In the present section the scatter in the natural frequencies of the reduced system is reported, due to the uncertainties in the launcher on one hand and in the satellite on the other hand.

2. *Uncertainties in the Launcher*

To compute the scatter in the natural frequencies due to uncertainties in the launcher, the COV of the uncertain input parameters of the launcher has been reduced to 5% of the value reported in Table 1. In other words, for the Young's moduli of isotropic materials, the COV was set to 0.4%. With the associated results a linear extrapolation has then been carried out. In Fig. 6 the COVs of the natural frequencies up to 50 Hz are shown. The scatter is rather modest, as the COVs are mostly below 4%. Only a few modes have COVs close to 10%, for higher frequencies up to 14%. In general, the scatter in the natural frequencies induced by uncertainties in the launcher is quite little.

Clearly, the extrapolation represents a linear approximation; hence, the accuracy deteriorates for larger deviations from the nominal values. Nevertheless, the obtained results are indicative for the magnitude of the scatter.

3. *Uncertainties in the Satellite Structure*

Figure 7 shows the COVs of the natural frequencies of the CB-reduced system, due to the uncertainties in the satellite. In this case the scatter is extremely small; in the range below 40 Hz all the COVs are less than 1% and many of them are practically zero. This is not

Table 1 Assumed coefficients of the variation of uncertain finite element model parameters

Element/material type	Property	COV (σ/μ)
Isotropic material	Young's modulus	8%
	Poisson's ratio	3%
	Shear modulus	12%
	Mass density	4%
Orthotropic shell element material	Young's modulus	8%
	Shear modulus	12%
	Mass density	4%
Solid element an-isotropic material	Material property matrix	12%
	Mass density	4%
Simple beam	Section dimension	5%
	Nonstructural mass	8%
Layered composite material	Nonstructural Mass	8%
	Thickness of plies	12%
	Orientation angle	$\sigma = 1.5$ deg
Shell element	Membrane thickness	4%
	Nonstructural mass	8%
Spring element	Stiffness	10%
Concentrated mass	Mass	3%
Damping	Modal damping	40%
	Structural damping	25%

surprising, because the satellite's structural mass is extremely small compared to that of the launcher; hence, the scatter in its properties is expected to have a rather small impact on the modal content of the coupled system.

F. Load Case 1: Liftoff (LO)

1. *General Remarks*

As the results presented in this section clearly show, the magnitude of the response scatter induced by the uncertainties in the FE model parameters depends on the response quantity under investigation. This applies, in particular, to the relative importance of the source of the uncertainties, that is, the launcher, the satellite, or the loading. Therefore in this paper results pertaining to two response quantities are presented, which exhibit scatter of quite different magnitude. The first one is the resultant force at the interface between the spacecraft and the launcher, shown in the left portion of Fig. 8; the second one is the von Mises stress in the solar panel hold-down beam (SPHB), depicted on the right in Fig. 8.

2. *Uncertainties in the Launcher Model*

In this section the scatter in the response is presented, due to the uncertainties in the parameters of the launcher model. In the left portion of Fig. 9, various percentiles of the resultant force at the interface between launcher and satellite are shown, for the time range

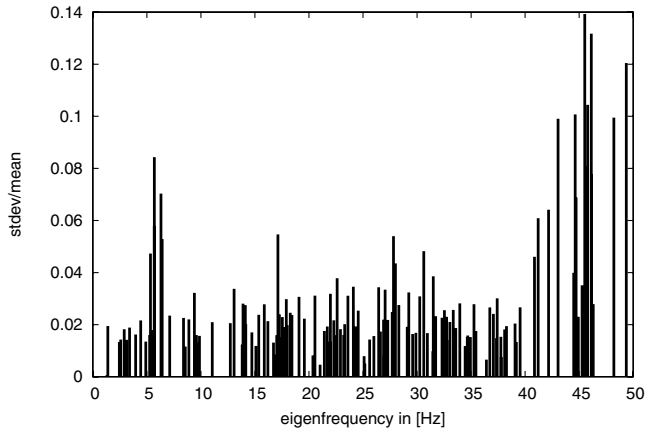

Fig. 6 Coefficients of variation of the eigenfrequencies of the assembled Craig–Bampton model vs frequency, due to scatter in launcher.

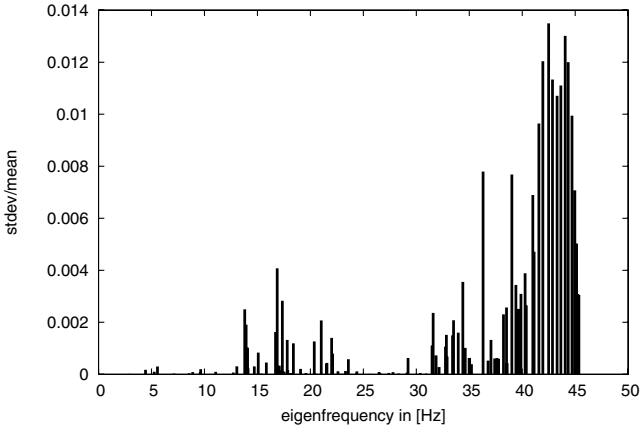

Fig. 7 Coefficients of variation of the eigenfrequencies of the assembled Craig–Bampton model vs frequency, due to scatter in satellite.

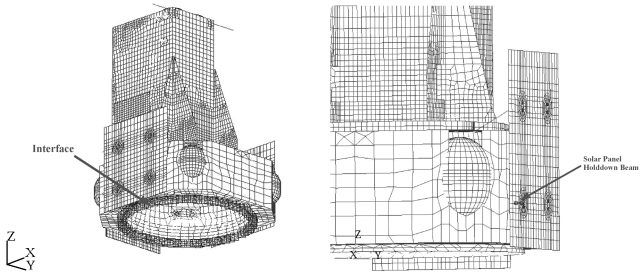

Fig. 8 Response quantities of interest: resultant interface force (left) and von Mises stress in SPHB (right).

between 0.0 and 0.35 s. For instance, the top cyan line denotes the level of the interface force that will be exceeded with a probability of 0.2%. The heavy black line denotes the response of the nominal FE model, that is, when all parameters are kept at their mean value. In fact, the nominal response and the 50% fractile are identical in this case. The scatter in the interface force is rather limited, as the lines denoting the fractiles are closely clustered around the nominal response. For 98.8% of the realizations the interface force is enclosed by the top (cyan) and the bottom (green) line. It should be noted that the entire ordinate is not displayed, but only the relevant portion. If the entire ordinate would be shown, the small magnitude of the scatter would be even more apparent.

In the right portion of Fig. 9 the response percentiles are shown for the von Mises stress in the SPHB. This response experiences a slightly larger scatter; again the percentiles are clustered almost symmetrically around the nominal response.

3. *Uncertainties in the Loading*

This section deals with the effect of uncertainties in the loading for the liftoff load case. The quantitative assumptions concerning the probabilistic modeling are based on [24] and are as follows:

1) Amplitude of pressure in EAPM and EAPP: A Gaussian probability function is assumed with a mean value of 1.15% above the deterministic amplitude and a standard deviation of 0.38% of the deterministic value of the amplitude.

2) Pressure levels of blast waves [duct 1 over pressure (DOP1) and duct 2 over pressure (DOP2)]: A Gaussian probability function is assumed with a mean value at the deterministic pressure level and a standard deviation of 3.3% of the deterministic value.

3) Time difference between ignition of the EAPM and EAPP boosters: The time delay of ignition of the EAPM booster is kept deterministic whereas for the time delay of the EAPP booster a Gaussian probability function is assumed with a mean value at the deterministic time delay (3.272 s) and a standard deviation of 8.3 ms.

Figure 10 shows on the left the percentiles of the resultant interface force, where the scatter is now due to the above described

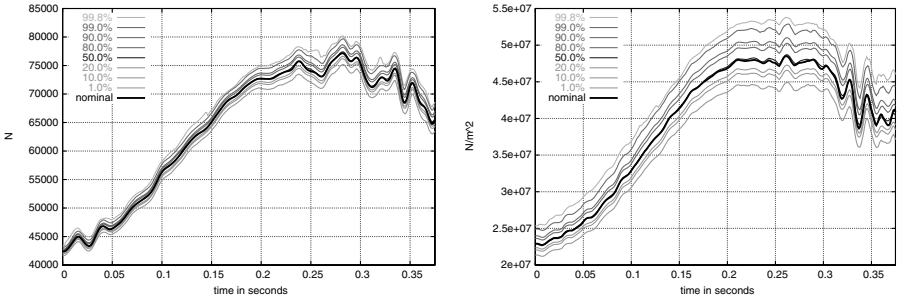

Fig. 9 LO load case, launcher scatter, response fractiles; left: interface force, right: von Mises stress in SPHB.

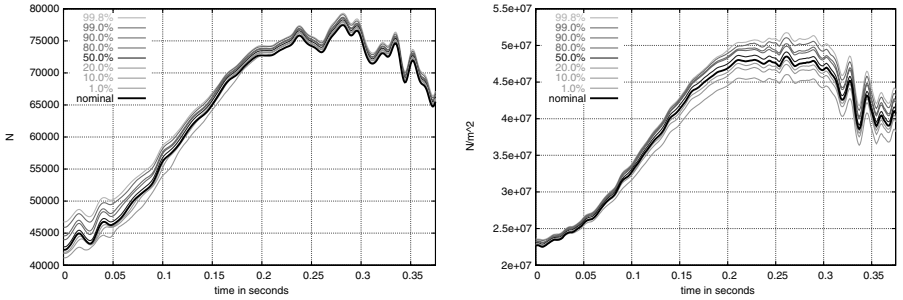

Fig. 10 LO load case, load scatter, response fractiles; left: interface force, right: von Mises stress in SPHB.

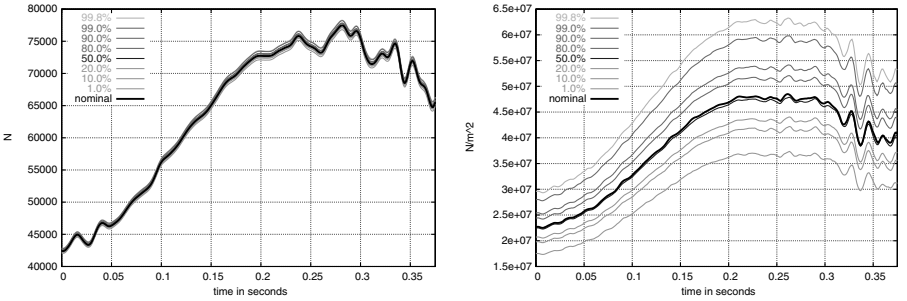

Fig. 11 LO load case, satellite scatter, response fractiles; left: interface force, right: von Mises stress in SPHB.

uncertainties in the loads. This figure should be compared with the left portion of Fig. 9, which represents the scatter due to uncertainties in the launcher structure. It can be observed that, in comparison, the load scatter induces a larger scatter in the initial phase of the transient response, which tends to disappear as time progresses. Furthermore, the nominal response (heavy black line) tends to become a lower bound to the interface force. This is due to the fact that for one of the force variables modeled as a random variable, namely, the pressure (thrust) level of the EAPM and EAPP component, the nominal value was equal to one of the 3σ bounds of the assumed normal distribution.

Comparing the right portions of Figs. 9 and 10, which relate to the von Mises stress in the SPHB, one can observe that in this case the load scatter has a minor impact in the initial phase, but as time progresses it results in a scatter of similar magnitude and shape.

4. Uncertainties in the Satellite Model

On the left of Fig. 11 the percentiles of the interface force between the satellite and the launcher during liftoff are shown for the case in which the uncertainties in the FE model parameters of the satellite have been modeled. Clearly, the scatter is very modest, which is consistent with the expectation that the scatter in the INTEGRAL, with its small contribution to the overall mass budget, has a limited impact on the overall response. This is, however, not the case for the von Mises stress in the SPHB, depicted on the right. This response quantity is affected strongly by the uncertainties in the satellite model, since the percentiles are quite spread out.

5. Relative Impact of Uncertainties in the Model of the Launcher and of the Satellite

The relative importance of the launcher scatter and the satellite scatter depends on the considered response quantity. The left portion of Fig. 12 compares the scatter in the interface force, due to the uncertainties in the launcher (heavy line, LS) and in the satellite (thin line). The mean response $\mu(t)$ (solid line) is depicted along with the $\mu + \sigma$ (dash-dotted line) and the $\mu - \sigma$ (dashed line) responses, where σ is the pertinent standard deviation. Hence the interval between the dashed and dash-dotted line can be viewed as the $[-\sigma, +\sigma]$ interval around the mean and gives a concise idea of the magnitude of the scatter. Clearly, for the interface force this interval is significantly larger in the case of launcher scatter (heavy line), implying that the uncertainties in the launcher have a greater impact on the scatter in the interface force.

However, if one considers the von Mises stress in the SPHB the situation is quite different, as the right part of Fig. 12 confirms. Here the $[-\sigma, +\sigma]$ interval around the mean, and hence the scatter, is greater in the case of the satellite scatter (thin lines).

6. Relative Impact of Uncertainties in the Model of the Loading and of the Satellite

The observation that the relative impact of the uncertainties depends on the response quantity under consideration can be extended to the comparison between the loading and the satellite. Concerning the interface force, shown in the left portion of Fig. 13, one can conclude that both the uncertainties in the loading and the in the satellite induce a negligible scatter. On the other hand, the

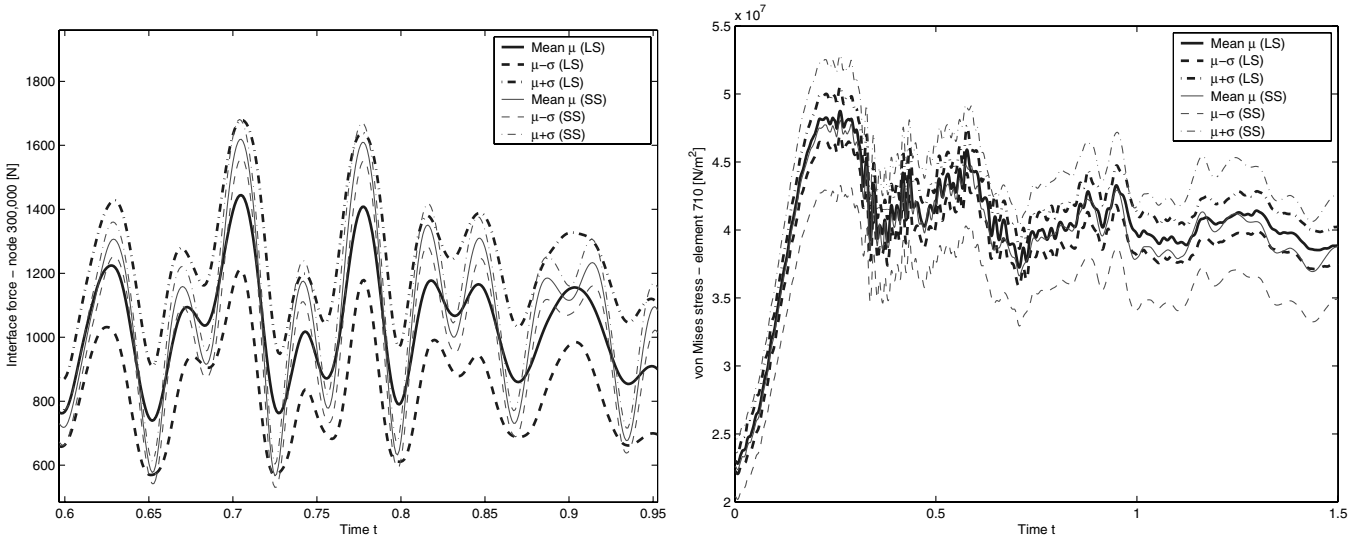

Fig. 12 LO load case, interface force, comparison launcher scatter (LS, heavy line) vs satellite scatter (SS, thin line); left: interface force (restricted time interval), right: von Mises stress in SPHB.

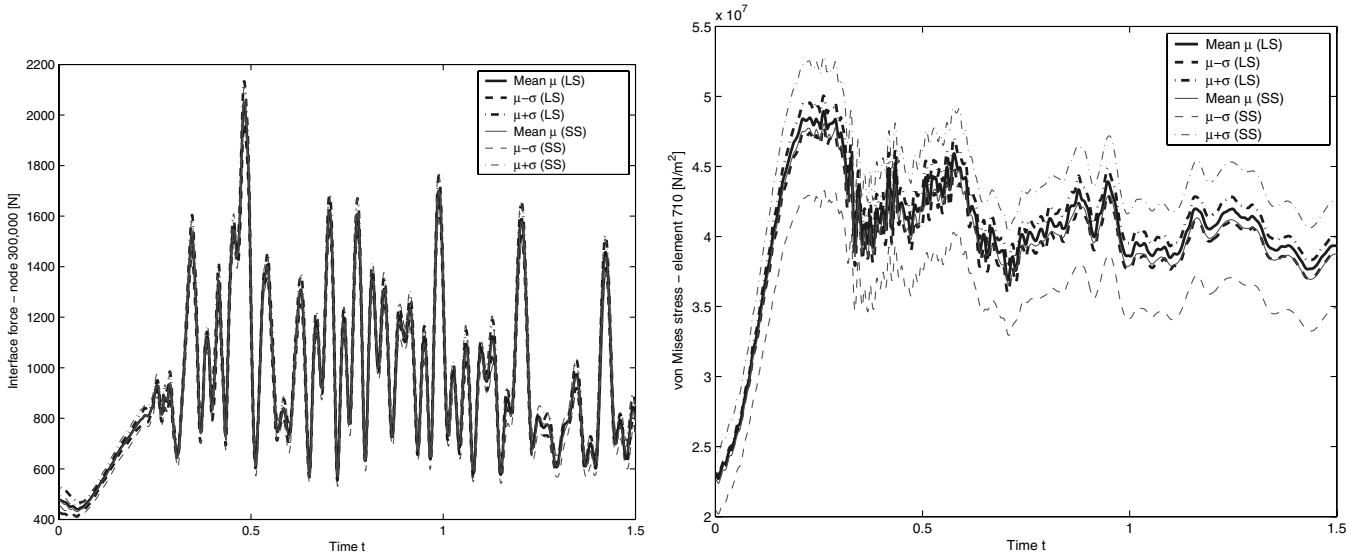

Fig. 13 LO load case, comparison load scatter (LS, heavy line) vs satellite scatter (SS, thin line); left: interface force, right: von Mises stress in SPHB.

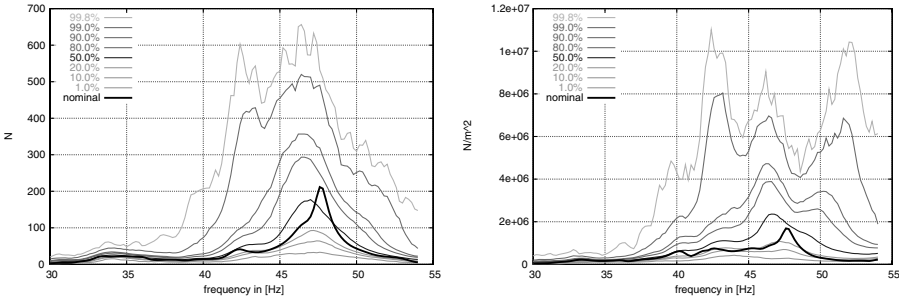

Fig. 14 EBP load case, launcher scatter, response fractiles; left: interface force, right: von Mises stress in SPHB.

von Mises stress in the SPHB is much more sensitive to scatter in the satellite's properties, as the right part of Fig. 13 reveals.

G. Load Case 2: End-of-Booster Pressure (EBP)

1. General Remarks

For this second load case the results of the response scatter lead to a similar observation as for the LO load case, namely, that the magnitude of the response scatter induced by the uncertainties is highly dependent on the considered response quantity. Therefore, for this load case, too, both the resultant of the interface force (left portion of Fig. 8) and the von Mises stress in the SPHB (right portion of Fig. 8) are considered.

2. Uncertainties in the Launcher Model

Figure 14 shows the frequency response in the range between 30 and 55 Hz, in terms of the interface force on the left and the von Mises stress in the SPHB on the right. As can be observed, in this case the

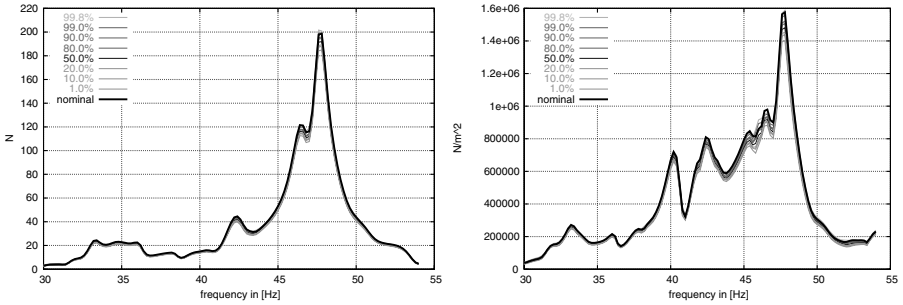

Fig. 15 EBP load case, load scatter, response fractiles; left: interface force, right: von Mises stress in SPHB.

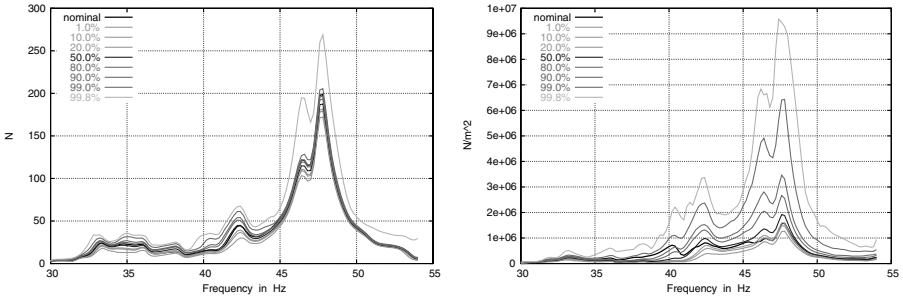

Fig. 16 EBP load case, satellite scatter, response fractiles; left: interface force, right: von Mises stress in SPHB.

scatter in both responses is enormous: the 99.8% fractile exceeds the nominal response by a factor of 3 for the interface force and more than a factor of 5 for the von Mises stress. This may be attributed to two different reasons: the shifting of the eigenfrequencies, due to the variations of stiffness and mass parameters, on one hand, and the scatter in the damping properties, on the other.

3. *Uncertainties in the Loading*

In this section the effect of uncertainties in the loading is discussed for the EBP load case. The quantitative assumptions concerning the probabilistic modeling are based on [25] and are as follows:

1) Amplitude of pressure perturbation in boosters EAPM and EAPP: A Gaussian probability function is assumed with the mean value at −5% of the deterministic pressure amplitude and a standard deviation of 1.7% of the deterministic pressure.

2) Phase shift between EAPM and EAPP pressure perturbations: The deterministic value is 180 deg (out of phase). A uniform probability density function for the phase shift in the interval (0 deg, 180 deg) is assumed.

Figure 15 contains the percentiles of the interface force and the von Mises stress in the SPHB. It turns out that for both considered response quantities the uncertainties in the loading have a negligible effect on the predicted response. Over most of the spectrum the various lines representing the percentiles are hardly perceivable. Only at the peaks can the lines be clearly distinguished.

4. *Uncertainties in the Satellite Model*

Figure 16 shows the percentiles of the frequency response in the range between 30 and 55 Hz, where the scatter is now caused by the uncertainties in the FE model of the satellite. For the interface force (left portion) the scatter is very modest over most of the frequency range; however, it is non-negligible in the vicinity of the peak frequency responses, in particular, at the main peak at approximately 47.5 Hz. Especially the 99.8 percentile is clearly distinct from the other percentiles. Again, the von Mises stress in the SPHB is more

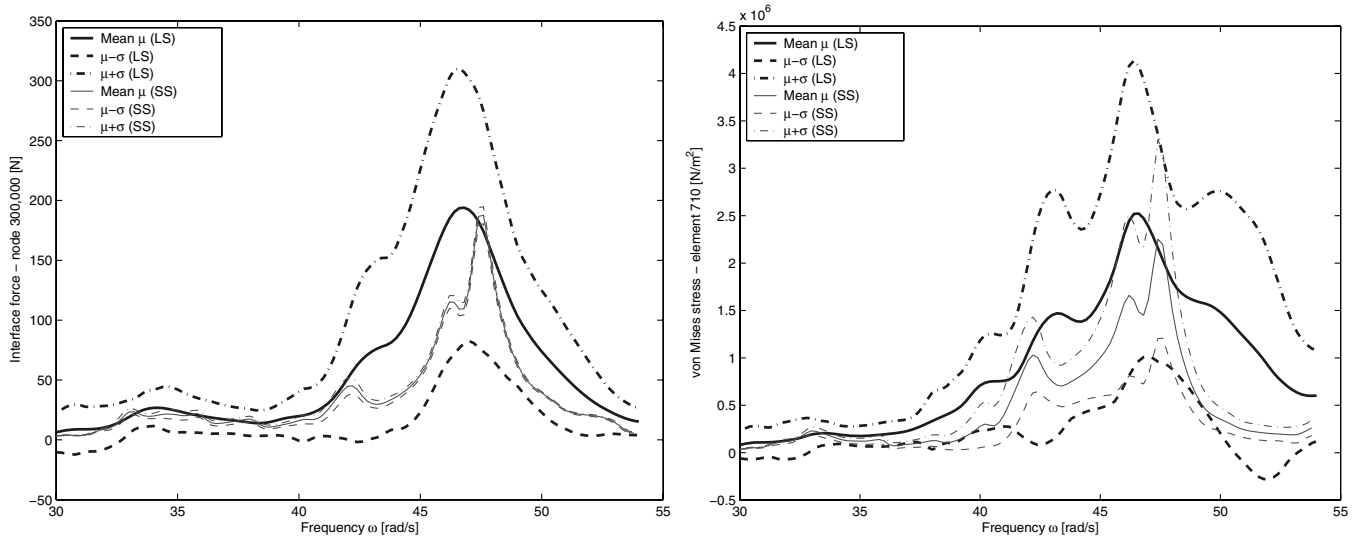

Fig. 17 EBP load case, comparison launcher scatter (LS, heavy line) vs satellite scatter (SS, thin line); left: interface force, right: von Mises stress in SPHB.

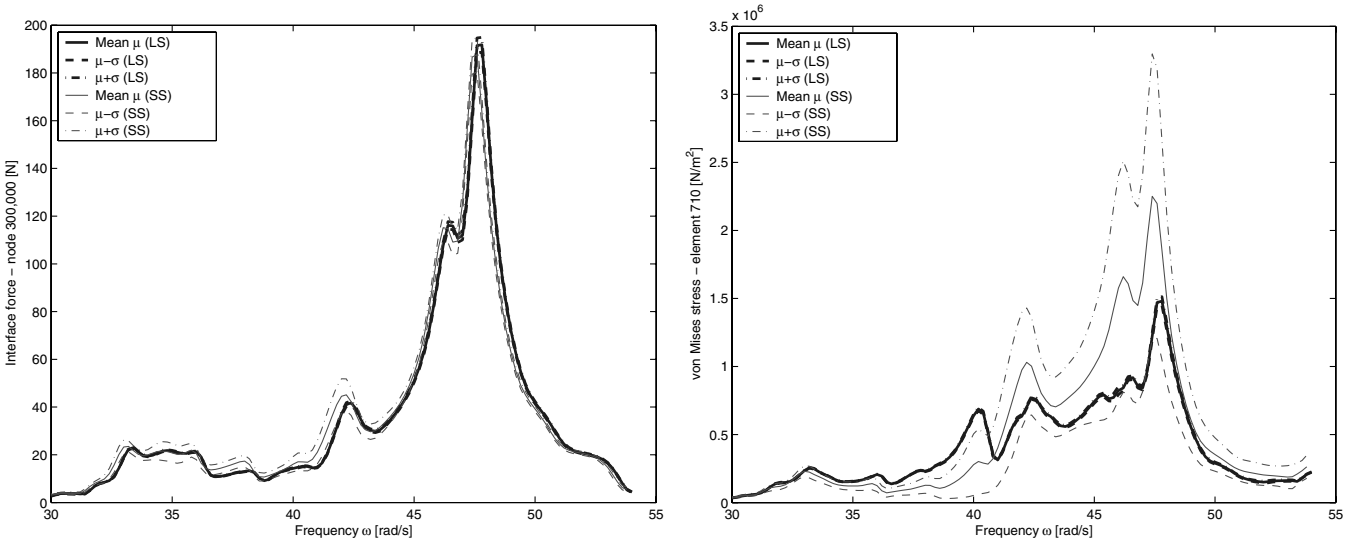

Fig. 18 EBP load case, comparison load scatter (LS, heavy line) vs satellite scatter (SS, thin line); left: interface force, right: von Mises stress in SPHB.

sensitive to uncertainties in the satellite's model parameters, as the right portion of Fig. 16 shows. In particular, the maximum stress occurring between 45 and 50 Hz exhibits enormous scatter: the 99.8% fractile exceeds the nominal response by a factor of more than 5.

5. Relative Impact of Uncertainties in the Model of the Launcher and of the Satellite

Compared with the LO load case, in the EBP load case the relative importance of the launcher scatter is clearly dominating with respect to the scatter in the satellite, as one can confirm by considering the $[-\sigma, +\sigma]$ interval around the mean, shown in Fig. 17. Both for the interface force and the von Mises stress the $[-\sigma, +\sigma]$ intervals are extremely wide in the case of the launcher scatter (heavy line). The satellite scatter, on the contrary, has a negligible effect on the interface force, but a strong influence on the von Mises stress of the SPHB. In summary, the results reveal that the launcher scatter has a significant effect on the global response, whereas the uncertainties in the satellite model have more of a localized impact.

6. Relative Impact of Uncertainties in the Model of the Loading and of the Satellite

Figure 18 allows an assessment of the relative importance of load scatter versus satellite scatter. Clearly, the uncertainties in the loading (thick lines) are basically negligible, as they can hardly be distinguished. The satellite scatter, although negligible with respect to the interface force, does induce a very strong scatter in the von Mises stress and thus cannot be neglected.

IV. Conclusions

In this paper the results of a full-scale uncertainty analysis for the coupled system launcher payload have been presented. To ensure generality and credibility of the uncertainty analysis, the basic strategy, underlying the probabilistic modeling process, was to consider the uncertainty in as many parameters of the FE model as possible. The uncertainties in the launcher model, in the satellite model, and in the loading have been analyzed separately, to preserve the ability to assess their relative impact.

Two load cases have been analyzed, namely, the liftoff load case in the time domain and the end-of-booster pressure oscillation load case in the frequency domain.

For the liftoff load case the considered responses, that is, the interface force and the von Mises stress in the solar panel hold-down beam showed "well-behaved" scatter. The deviation from the nominal solution is approximately symmetric and normally distributed and the coefficient of variation is on the order of 15–20%. The relative importance of the uncertainties in the launcher versus those in the satellite depends on the considered response quantity: for instance, the scatter in the interface force is larger in the presence of the launcher scatter; however, the opposite is true for the von Mises stress in the beam attaching the solar panels to the satellite structure, which is strongly influenced by the uncertainties in the satellite model. As far as the uncertainties in the loading are concerned, these turned out to have quite a minor impact on the response uncertainty, that is, under the assumptions made.

For the EBP load case, the scatter due to launcher scatter, is extraordinarily large. The coefficients of variation are well beyond 50%, the distribution is highly skewed, and the extreme values exceed the nominal value by factors of 3 or 4. For this load case the von Mises stress in the SPHB is also very sensitive to the uncertainties in the satellite model, whereas the latter affect the interface force only very little.

In summary, the results of this study show that the uncertainties in the FE models of the launcher and the spacecraft lead to uncertainties in the response quantities, which can be very large. The magnitude of this response scatter cannot be predicted a priori, which implies the necessity of performing uncertainty analyses similar to the one presented, in order to ensure the fitness of the designed structure. Neglecting these uncertainties can be dangerous, because strong sensitivities of some response quantities to the unavoidable uncertainty or variability of the model parameters would remain then undisclosed.

Clearly, the explicit consideration of uncertainties in the numerical analysis cannot act as a full substitute for testing and qualification campaigns; for instance, gross errors in the FE model would not be covered by the model, even if uncertainties are modeled and propagated.

Acknowledgments

This research is partially supported by the Austrian Research Council (FWF) under contract number P16769-N12, which is gratefully acknowledged by the authors. The supply of the FE model by ESA/ESTEC is also deeply appreciated.

References

[1] Calvi, A., "Uncertainty-Based Loads Analysis for Spacecraft: Finite Element Model Validation and Dynamic Responses," *Computers and Structures*, Vol. 83, No. 14, 2005, pp. 1103–1112.

[2] Esnault, P., and Klein, M., "Factors of Safety and Reliability—Present Guidelines and Future Aspects," *Proceedings of the Conference on Spacecraft Structures, Materials and Mechanical Testing*, SP-386, ESA, Nordwijk, The Netherlands, March 27–29 1996, pp. 109–119.

[3] Klein, M., Schuëller, G., Deymarie, P., Macke, M., Courrian, P., and Capitanio, R. S., "Probabilistic Approach to Structural Factors of Safety In Aerospace," *Proceedings of the International Conference on*

Spacecraft Structures and Mechanical Testing, Cépadués-Editions, Paris, France, 1994, pp. 679–693.

[4] Majed, A., Parting, K., Henkel, E., and Sarafin, T., "Variational Coupled Loads Analyses: Reducing Risk in Development of Space-Flight Hardware," *Journal of Spacecraft and Rockets*, Vol. 42, No. 1, 2005, pp. 98–104.

[5] Rubinstein, R., *Simulation and the Monte Carlo Method*, Wiley, New York, 1981.

[6] Bousquet, P., Mercier, F., and Klein, M., "Coupled Load Analysis: Scatter Related to Model Uncertainties," *Proceedings of the International Conference on Spacecraft Structures and Mechanical Testing*, SP-321, ESA, Noordwijk, the Netherlands, 1991, pp. 53–58.

[7] Mace, B., and Shorter, P., "A Local Modal/Perturbational Method for Estimating Frequency Response Statistics of Built-Up Structures with Uncertain Properties," *Journal of Sound and Vibration*, Vol. 242, No. 5, 2001, pp. 793–811.

[8] Craig, R., and Bampton, M., "Coupling of Substructures for Dynamic Analysis," *AIAA Journal*, Vol. 6, No. 7, 1968, pp. 1313–1319.

[9] Fransen, S., "Data Recovery Methodologies for Reduced Dynamic Substructure Models with Internal Loads," *AIAA Journal*, Vol. 42, No. 10, 2004, pp. 2130–2142.

[10] Craig, R., *Structural Dynamics—An Introduction to Computer Methods*, Wiley, New York, 1981.

[11] Notarnicola, M., Paron, A., Tizzani, L., and Evans, E., "INTEGRAL—Structural Mathematical Model Description and Dynamic Analysis Results," TR INT-TN-Al-0089, Issue 2, Alenia Aerospazio Space Division, Turin, Italy, April 15 1998.

[12] Ngan, I., *Ariane-5 FE Model Description Configuration*, ESA/ESTEC, Noordwijk, The Netherlands, 2000.

[13] Guyan, R., "Reduction of Stiffness and Mass Matrices," *AIAA Journal*, Vol. 3, No. 2, 1965, p. 380.

[14] Kreis, A., "FABE 2.6b User Documentation," Kreis Consultancies Technical Report, 2000.

[15] Fransen, S., "An Overview and Comparison of OTM Formulations on the Basis of the Mode Displacement Method and the Mode Acceleration Method," *Worldwide Aerospace Conference and Technology Showcase*, MSC.Software Corporation, Toulouse, France, April 8–10 2002, http://www.mscsoftware.com/events/aero2002.

[16] Fransen, S., Kreis, A., and Klein, M., "Pendulum Mode Control of Free-Free Launcher Structural Models in Gravity Fields," *Journal of Spacecraft and Rockets* (to be published).

[17] Golub, G., and Van Loan, C., *Matrix Computations*, 3rd ed., The Johns Hopkins University Press, Baltimore, 1996.

[18] Székely, G., Teichert, W., Brenner, C., Pradlwarter, H., Klein, M., and Schuëller, G., "Practical Procedures for Reliability Estimation of Spacecraft Structures and Their Components," *AIAA Journal*, Vol. 36, No. 8, 1998, pp. 1509–1515.

[19] Simonian, S., "Survey of Spacecraft Damping Measurements: Applications to Electro-Optic Jitter Problems," *The Role of Damping in Vibration and Noise Control*, Vol. DE-5, ASME, Fairfield, NJ, Sept. 1987, pp. 287–292.

[20] Schuëller, G., Pradlwarter, H., and Pellissetti, M., "Application of the Reliability Version of ASKA/NASTRAN, Work-packages 1000, 2000, 3000, 4000," Software Documentation 16144/02NL/PA, Institut für Mechanik, Universität Innsbruck, 2004.

[21] Fa. Lasso and Institut für Mechanik, Universität Innsbruck, *ASKA_RV Users Manual*, 1999.

[22] Institut für Mechanik, Universität Innsbruck, *NASTRAN_RV Users Manual*, 1999.

[23] Fransen, S., *Coupled Loads Analysis Toolbox V70.7 (dmap code for use with MSC.Nastran)*, ESA/ESTEC, Noordwijk, The Netherlands, 2003.

[24] Aerospatiale Matra Lanceurs, *Exploitation de Niveau 1 du vol 503—Restitution des Ambiances Dynamiques BF lors de la Phase de Decollage cas de Charge onde de Soufflé et Acoustique*, 18.11. 1999, issue 1, revision 1.

[25] Aerospatiale Matra Lanceurs, *Exploitation de Niveau 1 du vol 503—Restitution des Ambiances Dynamiques BF dues aux Oscillations de Pression EAP—1er et 2eme Modes Acoustiques*, 20.08. 1999, issue 1, revision 1.

L. Peterson
Associate Editor